Project 4: Interference

Gianfranco Grillo

November 2nd, 2017

Abstract

We present the results of a series of optical experiments performed to illustrate the wave nature of light via the phenomenon of interference. We use interference effects to measure the thickness of a cover glass, estimate the wavelength of the light from a HeNe laser, and measure the frequency separation of the laser's axial modes. We find good agreement between experimental and expected results, especially for the thickness of the cover glass and the frequency separation of the modes. The thickness of the cover glass with a nominal value of 0.43 mm was measured to be 0.451 ± 0.013 mm, and obtained a frequency separation of the modes of 1.33 ± 0.05 GHz, equivalent to a laser cavity length of 11.2 ± 0.4 cm, both of which consistent with the typical values of a tabletop HeNe laser. Although the wavelength of the laser could not be measured very accurately, we were able to verify that it is in the order of the hundreds of nanometers, as expected. Finally, we were able to observe the interference pattern of a Fabry-Perot interferometer, although the way the pattern changed when the incident laser light was filtered by a polarizer at different angles was not totally consistent with expectations.

1 Introduction

The question of what kind of scientific model is able to most accurately describe the nature of light has a long and illustrious story. For a long time, in part due to the influence of Newton, light was believed to consist in nothing more than a stream of particles, in what was known as the corpuscular theory of light. Robert Hooke, one of Newton's most despised rivals, was a proponent of the theory that light was actually a wave, but his views did not become popular until long after his death, due to the discovery of the phenomena of interference and diffraction in the 19th century, and the development of classical electromagnetism by Maxwell. Although later developments demonstrated that this wave model does not consitute the whole picture, it has a remarkable range of validity, and is the cornerstone of classical optics.

In this project, we use simple experimental setups and laboratory equipment in order to perform a series of experiments illustrating the phenomenon of interference, and use interference effects to measure the thickness of a cover glass and the frequency separation of the axial modes of a laser. We construct two types of classical interferometers, the Michelson interferometer and the Fabry-Perot interferometer, the former of which we use to measure the frequency separation of the modes. Where appropriate, we apply geometrical optics and the thin lens approximation in order to derive our results.

We perform the data analysis using Python and the associated libraries NumPy and SciPy ([1]), as well as the Uncertainty package ([2]).

2 Theoretical background

2.1 Thickness Measurement by Interference

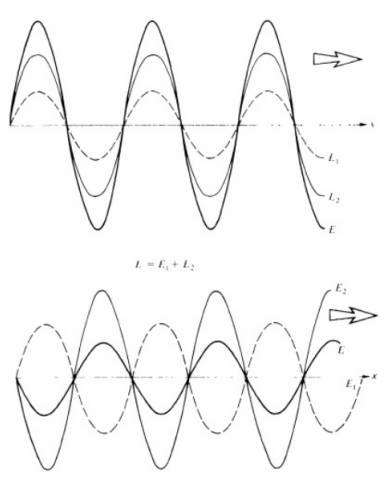

Figure 1: Constructive and destructive interference of two waves. Obtained from [3].

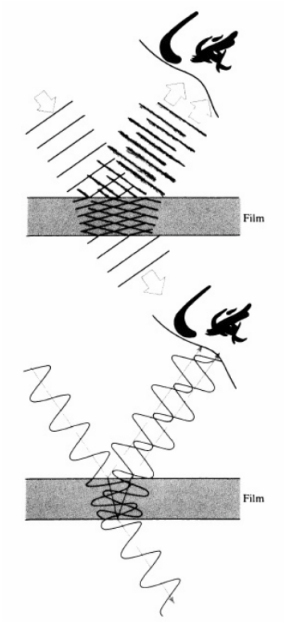

Figure 2: Interference due to a thin film. Obtained from [3].

The phenomenon of wave interference can be described mathematically by the addition of two or more sinusoids. Depending on the relative phase of the sinusoids, their addition results in constructive or destructive interference. Figure 1 depicts the two simplest cases of complete constructive interference, which occurs when the waves are exactly in phase, and complete destructive interference, when the waves are exactly out of phase. Any phase difference in between these two extremes will result in partial interference.

A common way to produce interference effects using a single beam of coherent light, like the one produced by a laser, is to divide the beam into two parts and make one part travel a longer path than the other, at which point the beams are recombined and interference effects can be observed because the path length difference results in a phase difference between the two beams. This concept is behind the observed interference due to reflection of a thin film, as illustrated in Figure 2. A wave incident on the film is partially reflected and partially transmitted at the first interface, and the transmitted wavefront is then partially reflected and partially transmitted at the second interface. The reflected component at the second interface, in turn, is then partially reflected and partially transmitted as it hits the first interface from the opposite direction. The transmitted component of this wave then proceeds to interfere with the reflected component of the original wave, which results in the creation of interference fringes at a surface that is placed in the path of propagation of the reflection. For the

case of a thin film in air, the location of the bright fringes is given by (using $n_{air} \approx 1$)

$$\cos\theta_t = \frac{(2m-1)\lambda_0}{4nd} \tag{1}$$

where θ_t corresponds to the angle of transmission of the incident light with respect to the surface normal, λ_0 corresponds to the wavelength of the light in vacuum, n is the refractive index of the film, d is the film's thickness, and m is an integer that represents the order of the fringe. By Snell's Law, we have that

$$\sin\theta_i = n\sin\theta_t \tag{2}$$

Squaring and using the identity $\sin^2\theta = 1 - \cos^2\theta$, we can write this as

$$\cos\theta_t = \left(1 - \frac{\sin^2\theta_i}{n^2}\right)^{1/2} \tag{3}$$

Combining this with (1) and solving for $\sin^2\theta_i$ yields

$$\sin^2\theta_i = n^2 - \left[\frac{(2m-1)\lambda_0}{4d}\right]^2 \tag{4}$$

This equation indicates that it is possible to measure the thickness of a thin film by finding the angles θ_i that separate fringes of different orders. We will use this method in experiment 1 in order to measure the thickness of a cover glass.

2.2 Young's Double Slit Experiment and Lloyd's Mirror

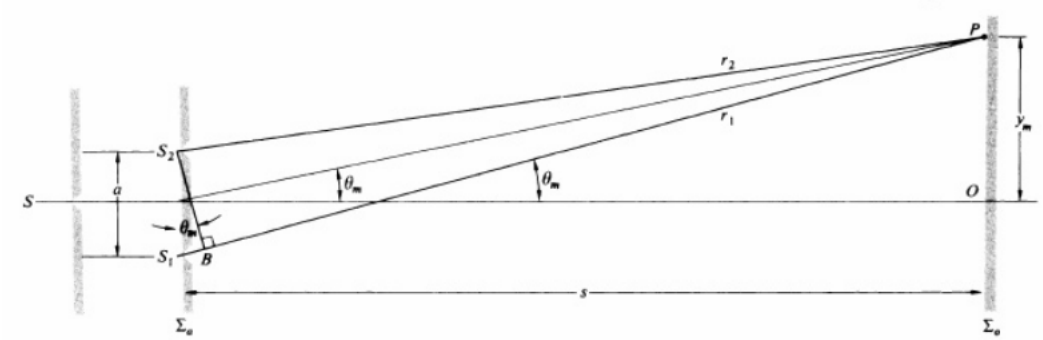

Figure 3: Geometry of Young's double slit experiment. Obtained from [3].

Perhaps the most famous interference experiment is the one first performed by the English scientist Thomas Young in the beginning of the 19th century. Light from a point source is incident upon a screen with two small apertures separated by a distance a, essentially dividing the incident wave into two individual point sources with no initial phase difference. Another screen is placed a distance s away from the first screen, where it is possible to observe fringes that are produced due to the difference in path length between the light coming from the two sources. The geometry of the experiment is

reproduced in Figure 3. If $s \gg a$, we can use the small angle approximation $\sin\theta \approx \theta$ and express the spacing of the fringes Δy as

$$\Delta y = \frac{s\lambda}{a} \tag{5}$$

where λ corresponds to the wavelength of the incident light. This means that if we measure the values of s, a, and Δy, we can determine λ, as (5) can be written as

$$\lambda = \frac{a\Delta y}{s} \tag{6}$$

An alternative way to reproduce the kind of geometry depicted in Figure 3 is by using a mirror instead of screen with two apertures. This is particularly well suited to the case in which the incident light is from a laser, because the beam width is very small and as such the apertures on the screen would have to be extremely close together in order for the light to actually pass through both of them. Instead, if a mirror is placed in the beam's path at a very small angle, we can recreate Young's experiment as the original, non-reflected beam interferes with the reflected beam in the same way that the two point sources in the original experiment interfere with each other. This arrangement is known as Lloyd's mirror, in honor of the Irish physicist Humphrey Lloyd, who invented it. The main practical difference with respect to the original double slit experiment is that the mirror introduces a phase shift of 180° on the incident light, so the light from the two sources starts out exactly out of phase instead of exactly in phase as it does in the original experiment. This implies that bright fringes in Lloyd's mirror correspond to bright fringes in the double slit configuration, but it does not affect the fringe separation, which is what we rely on in order to measure the light's wavelength. We will construct Lloyd's mirror in experiment 2 of this project and use it to measure the wavelength of a laser's beam.

2.3 Michelson Interferometer

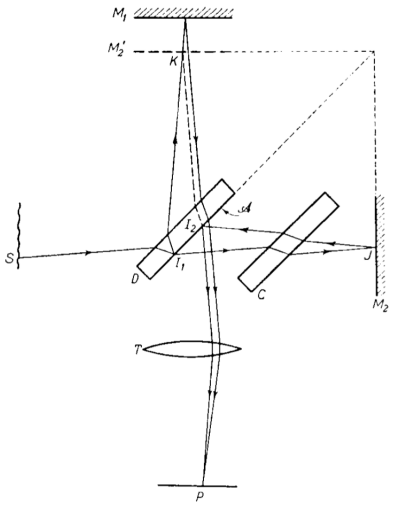

Figure 4: Illustration of the setup of a Michelson interferometer. Obtained from [4].

Another way to get a beam of light to interfere with itself is via the use of a configuration of optical devices commonly known as the Michelson interferometer, after the American physicist Albert A.

Michelson. A beam of light is incident on a beam splitter, where it is divided into two beams that travel at right angles with respect to each other. Two flat mirrors that face the beam splitter are placed such that they reflect each of the beams back towards the beam splitter, where they are both transmitted in the same direction. By adjusting the length of each of the arms of the interferometer, one can introduce a phase difference between the two beams that becomes apparent once they recombine. Because one of the beams passes through the beam splitter three times, and the other passes through it only once, it is common practice to introduce a compensating plate made of a transparent material in the propagation path of the second beam, in order to correct for this path difference, and make it depend exclusively on the relative position of each of the mirrors. It is also possible to place a converging lens before the beam stopper in order to bring the two beams into focus. This arrangement is shown in Figure 4. If a photosensor is placed at the beam stopper (P in the figure), the measured intensity is given by

$$I = I_1 + I_2 + 2\sqrt{I_1 I_2}\cos\delta \tag{7}$$

where I_1 and I_2 correspond to the intensity of each of the beams, and δ is the phase difference, which is related to the lengths of each of the arms l_1 and l_2 by the equation

$$\delta = \frac{4\pi c}{\nu_0}(n_1 l_1 - n_2 l_2) \tag{8}$$

where n_1 and n_2 correspond to the refractive indices of the medium constituting each of the interferometer arms, and ν_0 corresponds to the frequency of the light in vaccum. For the case of an interferometer that uses a 50/50 beam splitter, and where the beams propagate through air, we can write the intensity as

$$I = I_0\left[1 + \cos\left(\frac{4\pi c}{\nu_0}(l_1 - l_2)\right)\right] \tag{9}$$

Changing the position of either of the mirrors by Δx results in a change in the intensity given by

$$I = I_0\left[1 + \cos\left(\frac{4\pi c\Delta x}{\nu_0}\right)\right] \tag{10}$$

For the case of light that is not completely monochromatic, as is the case of laser light, the intensity curve is more complicated, since the different frequencies interfere to produce a beat effect. For the particular case of the laser beam used in this project, we expect there to be two axial modes of equal polarization separated by a frequency $\Delta\nu$, that will interfere with each other. In that case, we can derive the intensity measured by the photodetector by regarding the laser light as a superposition of two monochromatic waves, each one corresponding to one of the modes of oscillation. This implies that the interference now happens between four different waves. The electric field at the photosensor is then

$$E = E_1 + E_2 + E_3 + E_4 \tag{11}$$

The intensity is proportional to the square modulus of this sum,

$$\begin{aligned} |E|^2 &= (E_1 + E_2 + E_3 + E_4)(E_1^* + E_2^* + E_3^* + E_4^*) \\ &= |E_1|^2 + |E_2|^2 + |E_3|^2 + |E_4|^2 + 2Re(E_1E_2^*) + 2Re(E_1E_3^*) \\ &\quad +2Re(E_1E_4^*) + 2Re(E_2E_3^*) + 2Re(E_2E_4^*) + 2Re(E_3E_4^*) \end{aligned} \tag{12}$$

Following [5], we can write the time-averaged electric fields as

$$\begin{aligned} E_1 &= E_{01}e^{ik_1 x} \\ E_2 &= E_{01}e^{ik_1(x+2\Delta x)} \\ E_3 &= E_{02}e^{ik_2 x} \\ E_4 &= E_{02}e^{ik_2(x+2\Delta x)} \end{aligned} \tag{13}$$

where $k = \frac{2\pi}{\lambda}$, the wavenumber of the mode. Substituting into (12), and after performing some trigonometric algebra, we get

$$\begin{aligned} |E|^2 &= 2\left[E_{01}^2 + E_{02}^2 + E_{01}^2\cos(2k_1\Delta x) + E_{02}^2\cos(2k_2\Delta x)\right. \\ &\quad \left. +4E_{01}E_{02}\cos(k_1\Delta x)\cos(k_2\Delta x)\cos((k_1-k_2)(\Delta x+2x))\right] \end{aligned} \tag{14}$$

We define $a = \frac{E_{01}}{E_{02}}$, and rewrite this as

$$\begin{aligned} I \propto \frac{1}{2}\left|\frac{E}{E_{02}}\right|^2 &= 1 + a^2 + a\cos(2k_1\Delta x) + \cos(2k_2\Delta x) \\ &\quad +4a\cos(k_1\Delta x)\cos(k_2\Delta x)\cos((k_1-k_2)(\Delta x+2x)) \end{aligned} \tag{15}$$

The $2x$ factor in the last term is just an offset that does not affect the shape of the curve, so we can set $x = 0$. Rewriting in terms of ν_0 and $\Delta\nu$, we have that

$$\begin{aligned} I &\propto 1 + a^2 + a\cos\left(\frac{4\pi\nu_0\Delta x}{c}\right) + \cos\left(\frac{4\pi(\nu_0+\Delta\nu)\Delta x}{c}\right) \\ &\quad +4a\cos\left(\frac{2\pi\nu_0\Delta x}{c}\right)\cos\left(\frac{2\pi(\nu_0+\Delta\nu)\Delta x}{c}\right)\cos\left(\frac{2\pi\Delta\nu\Delta x}{c}\right) \end{aligned} \tag{16}$$

The frequency separation of the laser modes depends on the length L of the laser cavity, and is given by the simple expression

$$\Delta\nu = \frac{c}{2L} \tag{17}$$

For an HeNe laser with nominal wavelength $\lambda_0 = 632.8$ nm, and cavity length $L = 10$ cm, we have that $\nu_0 = 4.74 \times 10^{14}$ Hz and $\Delta\nu = \frac{c}{2L} = 1.50 \times 10^9$ Hz. Figure 5 shows a plot of (16) after normalization, using these values, and $a = 1$. As can be seen, the distance between the peaks of the modulating sinusoid corresponds to the length of the laser cavity. In practice, it is very difficult to experimentally recreate such a curve, because the high frequency of the light implies that the oscillations in the intensity are extremely sensitive to changes in Δx. For this reason, if the goal is to experimentally determine $\Delta\nu$, it is more convenient to do so by constructing a so called visibility curve. The interference effects give rise to a fringe pattern, and a measure of the contrast of this pattern is the visibility, which is defined as

$$\mathcal{V} = \frac{I_{max} - I_{min}}{I_{max} + I_{min}} \tag{18}$$

Essentially, this is a measure of the difference in intensity between the contiguous minima and maxima of the intensity curve. Obtaining a general formula for the visibility as a function of Δx is not as straightforward as obtaining the one for the intensity, especially if the relative intensities of the modes is not known. Figure 6 shows visibility curves for different kinds of quasimonochromatic light. A more detailed treatment of this topic is outside the scope of this work, and can be found in chapter

VII of [4]. For the purposes of this project, it is enough to say that if the difference in the relative mode intensities is large enough, we expect the visibility curve at some distance away from $\Delta x = 0$ to be well approximated by a damped sinusoid, that is,

$$\mathcal{V}(\Delta x) \approx \alpha e^{-\beta \Delta x} \sin(\gamma \Delta x + \epsilon) + \eta \tag{19}$$

where α, β, γ, ϵ, and η are free parameters that depend on the intensities of the modes and on $\Delta\nu$. We explicitly write $\Delta\nu$ in terms of γ as

$$\Delta\nu = \frac{c\gamma}{16\pi} \tag{20}$$

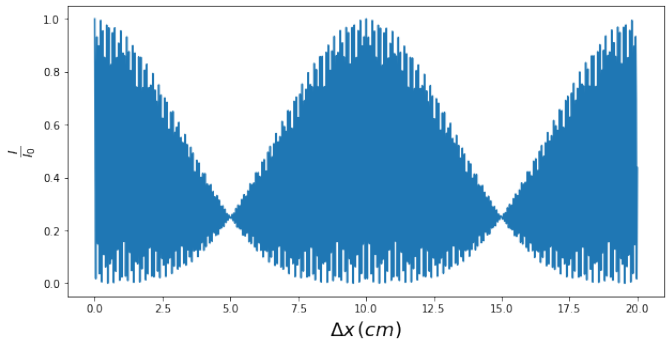

Figure 5: Intensity curve for the quasimonochromatic Michelson interferometer with $\nu_0 = 4.74 \times 10^{14}$ Hz and $\Delta\nu = 1.50 \times 10^9$ Hz.

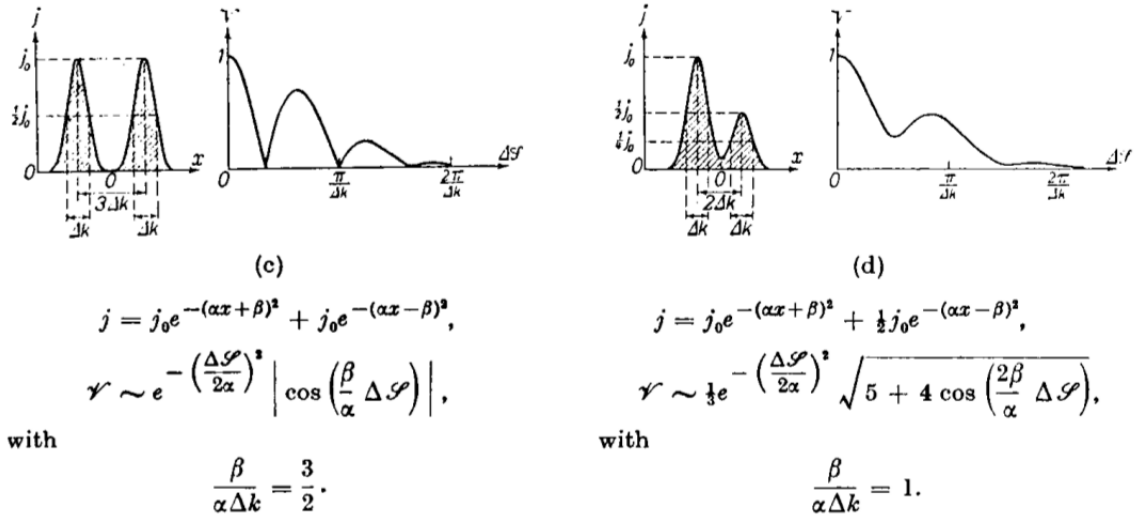

Figure 6: Visibility curves for two quasimonochromatic sources, with intensity profiles similar to those produced by a laser. Note that the path difference Δx is represented here as $\Delta\mathscr{S}$ instead. Obtained from [4].

2.4 Fabry-Perot Interferometer

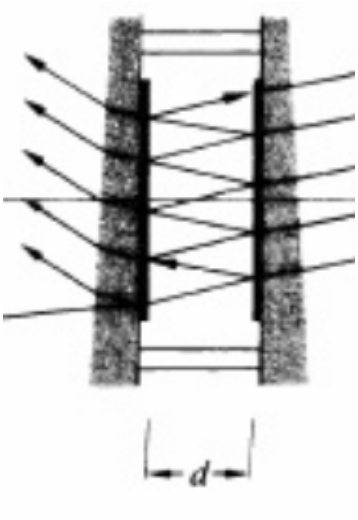

Figure 7: Cavity of a Fabry-Perot interferometer. Obtained from [3].

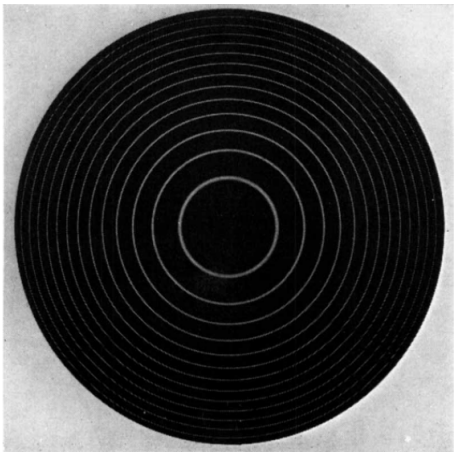

Figure 8: Fabry-Perot fringes. Obtained from [4].

The Fabry-Perot interferometer is an example of an interferometer that relies on multiple beam interference. Light that is incident on a parallel configuration of semi-transparent mirrors separated by a distance d undergoes multiple reflections as it bounces back and forth between the mirrors, as shown in Figure 7. Placing a viewing screen some distance away from the cavity allows one to observe circular interference fringes that are produced by the interference of the waves that are transmitted by the mirror. And idealized illustration of the fringes is shown in Figure 8. This type of interferometer is very useful for determining the frequency composition of light. Monochromatic light produces fringes like the ones shown in Figure 8. Light composed of different frequencies, on the other hand, shows up as multiple sets of fringes, one set each per frequency component. The interferometer's ability to resolve different frequencies is related to a quantity referred to as the finesse, which is in turn related to the Fabry-Perot interferometer's reflectivity. The finesse is defined as

$$\mathcal{F} = \frac{\pi\sqrt{F}}{2} \tag{21}$$

where F is known as the coefficient of finesse and is given by

$$F = \frac{4R}{(1-R)^2} \tag{22}$$

with R corresponding to the interferometer's power reflection coefficient. The minimum resolvable frequency separation $(\Delta\nu)_{min}$ between light components is then

$$(\Delta\nu)_{min} = \frac{c}{2\mathcal{F}nd} \tag{23}$$

where n is the refractive index of the medium located in between the parallel mirrors. A related quantity, the free spectral range $(\Delta\nu)_{FSR}$, corresponds to the frequency difference at which two sets of circular fringes overlap, and is given by

$$(\Delta\nu)_{FSR} = (\Delta\nu)_{min}\mathcal{F} = \frac{c}{2nd} \tag{24}$$

A more detailed examination of the properties of the Fabry-Perot interferometer can be found in chapter 9 of [3] and chapter VII of [4].

3 Experimental Set-Up and Results

3.1 Experiment 1

3.1.1 Set-Up

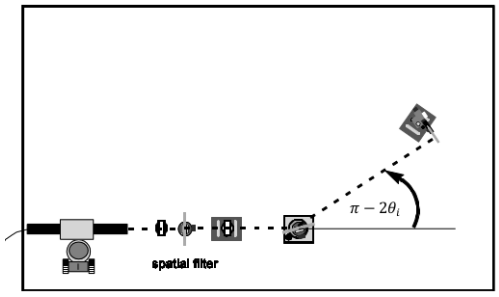

Figure 9: Setup for experiment 1. Obtained from [5].

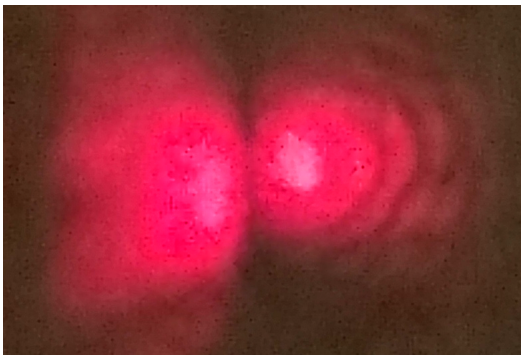

Figure 10: Image of the reflected beam when the dark fringe is at the center.

In this experiment, we measure the thickness of a cover glass by examining its reflection. We start by building a beam expander using 25 and 50 mm lenses, and a pinhole placed 25 mm away from the first lens in order to produce a point source. We now mount the cover glass into a filter holder placed on top of a rotation stage, and locate a beam stopper in a position appropriate to look at the beam reflected off the cover glass. We then rotate the stage until a dark interference fringe can be seen in the center of the reflection (Figure 10). We record the angle at which this occurs, and rotate the stage until we observe the same fringe configuration. We repeat this procedure a number of times to obtain multiple data points.

3.1.2 Results and analysis

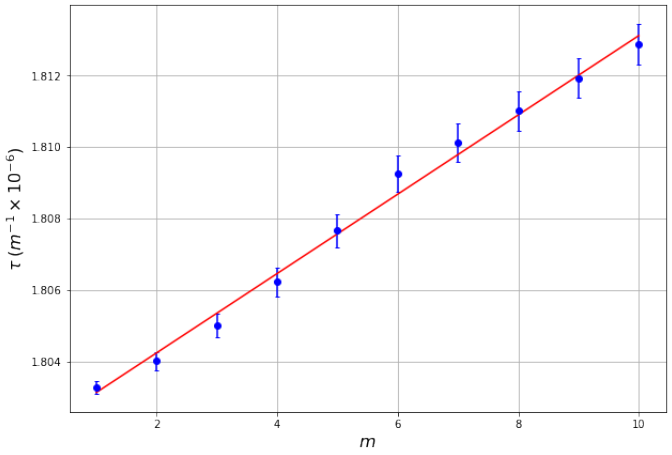

Figure 11: τ as a function of m, with experimental measurements and the fit model given in (25).

We rearrange equation (4) as

$$\tau = \frac{\sqrt{n^2 - \sin^2\theta_i}}{\lambda_0} = \frac{2m + \phi - 1}{4d} \tag{25}$$

where we have added an offset ϕ since the first fringe that appears in our measurements does not correspond to the first order fringe $m = 1$, but to an unknown order that cannot be calculated a priori. We then fit for the parameters m and d. We calculated the incident angle by using the relationship $\theta_m = \pi - 2\theta_i$, where θ_m is the angle that was actually measured (see Figure 9). This angle, in turn, was measured by measuring the x and y distances from the cover glass to the location of the spot in the beam stopper, in order to obtain a greater precision. We assume a standard error of $\Delta x = 0.3$ breadboard holes and $\Delta y = 0.1$ breadboard holes, where the x error is larger than the y error because the beam stopper was translated along the x-direction but not the y-direction. We obtain a best fit value for the thickness $d = 0.451 \pm 0.013$ mm, which is within 5% of the thickness value given by the manufacturer of $d = 0.43$ mm. The angles separating each fringe order was very small, and became smaller as the order of the fringe increased, with a separation for the last two fringes of less than 0.70°, which implies that very small errors in measuring the angles could have large effects on the results. Thus, the agreement with the manufacturer's value is quite remarkable given the simple procedure used to measure the angular separations.

3.2 Experiment 2

3.2.1 Set-Up

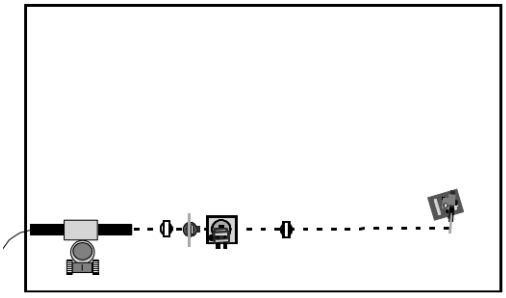

Figure 12: Setup for experiment 2. Obtained from [5].

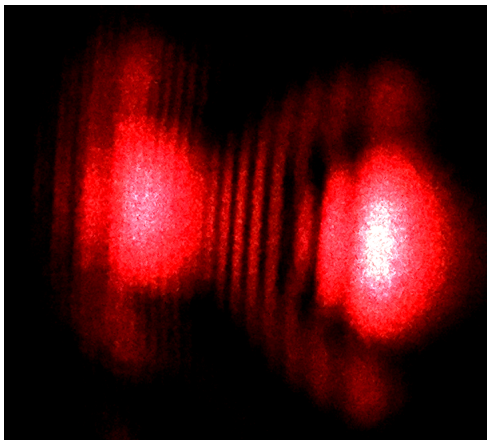

Figure 13: Image of the interference fringes in the Lloyd's mirror setup.

This experiment uses the Lloyd's mirror technique to recreate Young's double slit experiment without the need to use a screen with two apertures. We set up a spatial filter using a 25 mm lens to focus the laser light into a pinhole located at its focal distance. We now mount a mirror in a rotation stage a small distance away from the spatial filter and rotate it such that the incident light is incident on the mirror at an angle close to 90° with respect to the mirror's surface normal. Careful rotation of the mirror into this position enables the transformation of a single point source into two point sources. Next, we place a 40 cm lens at a distance $d_o > 40$ cm from the mirror, and place a screen at a distance d_i from the lens corresponding to the mirror's image plane, which is related to d_o and f by the thin lens equation, $1/d_i = 1/f - 1/d_o$. We now measure the separation a' between the two point sources at the screen, and use this to find the source separation $a = \frac{a' d_0}{d_i}$. Finally, we remove the 40 cm lens in order to obtain the interference pattern at the screen and measure the separation of the vertical fringes Δy. A diagram of the setup is shown in Figure 12, and a picture of the interference fringes is shown in Figure 13.

3.2.2 Results and analysis

Based on our description of the procedure above, if we take the screen to be at a distance $s = d_o + d_i$ from the mirror, we can write equation (6) as

$$\lambda = \frac{a\Delta y}{s} = \frac{a'\Delta y(d_o - f)^2}{d_o f^2 + d_o f(d_o - f)} \tag{26}$$

where we have used the thin lens equation to write d_i in terms of d_o and f, and a in terms of a', d_o, and f, in order to write the equation in terms of the experimentally measured quantities. We used a d_o of 61.5 ± 0.5 cm and a focal length $f = 40.0 \pm 0.1$ cm, and the measured source separation was

$a' = 1.0 \pm 0.5$ mm. The fringe separation was measured to be $\Delta y = 1.0 \pm 0.5$ mm. This gives a value for the wavelength of $\lambda = 306 \pm 300$ nm.

The error between this result and the expected value of the wavelength of 632.8 nm is big, and the standard error of the derived result is big too, on the same order as the nominal value. The reason for this is mainly that the measured values for a' and Δy have a large degree of uncertainty, because the distances were on the order of the minimum scale separation of the intrument used to measure them, a ruler. Slightly altering the value of either a' or Δy results in large changes in the value of λ. For instance, if a' where to change from 1.0 ± 0.5 mm to 1.5 ± 0.5 mm, the value of the wavelength becomes 687 ± 460 nm, and reducing the uncertainty in the measurement to 0.1 mm gives $\lambda = 687 \pm 90$ nm, which is much closer to the expected value than what we obtain with the measurements actually made. Thus, the derived value for the wavelength using this particular experimental procedure is not to be taken literally, and instead provides an order of magnitude estimate. Much better results can potentially be obtained by measuring a' and Δy using more accurate instrumentation and procedures.

3.3 Experiment 3

3.3.1 Set-Up

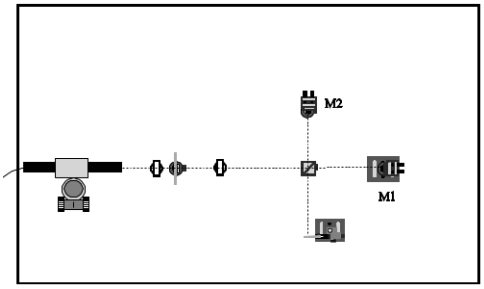

Figure 14: Setup for experiment 3. Obtained from [5].

In this part of the project, we construct a Michelson interferometer and perform some qualitative observations. We start by constructing a point source and a beam expander, in a similar manner as in experiment 1, but now using a 25 mm lens, a pinhole, and a 40 cm lens. We position a mirror M1 on a translation stage 40 cm away from the second lens, and a beam splitter in between the lens and the mirror at a distance of 15 cm from the mirror. We place another identical mirror M2 at a fixed distance of 15 cm away from the beam splitter at an angle of 90° with respect to M1, and a beam stopper at the other side of the beam splitter opposite M2. A diagram of the setup is shown in Figure 14. We now align our configuration such that interference fringes appear at the beam stopper, and perform some qualitative observations. We look at what happens to the fringes when we move the 40 cm lens towards the first lens, when we blow the Airoduster with its nozzle in one of the interferometer's arms, when we insert a finger into one of the arms close to the propagating beam, and when we push M1, the test mirror.

3.3.2 Results and analysis

In the starting configuration, the combination of the 25 mm lens and the pinhole transforms the laser beam into a point source that is then collimated by the 40 cm lens. If M1 is placed at a 40 cm distance

from this lens, the beam achieves its minimum radius at M1. Moving the lens towards the pinhole means that the light that emerges from the mirror is no longer collimated, and the minimum beam radius no longer occurs at M1. This should result in a variation in the spot diameter at the beam stopper. This effect, however, is very hard to detect because the spatial filter creates a very narrow beam. A more noticeable effect is that the fringes that show up at the beam stopper move as the lens changes position. This occurs because the lens introduces a phase shift on the wave front, and moving the lens implies that this shift is introduced at different positions along the path. We can also observe the fringes rounding up as the curvature of the wavefront at the mirror is increased.

Blowing the Airoduster with a nozzle inserted in one of the arms results in a blurring of the interference fringes at the beam stopper. From equation (8), we know that the phase difference between the beams depends in part on the refractive index of the medium constituting the interferometer's arms, and blowing the Airoduster results in variations on one of the refractive indices. Furthermore, the rapid flow of the gas emerging from the Airoduster implies that the refractive index in the arm is rapidly varying, which means that the phase difference is rapidly varying, which in turn results in the blurring of the interference fringes at the beam stop. This is different from shadowgraphy because the change in the structure of the interference fringes is directly sensitive to the value of the refractive indices in the interferometer's arms, whereas in shadowgraphy the changes in the observed patterns are proportional to either the first or second derivatives of the refractive index, depending on the configuration of the shadowgraph. Inserting a finger into one of the arms close to the path of beam propagation results in a similar effect, as the warm air from the finger alters the refractive index of the arm.

Pushing the test mirror results in the fringes at the beam pattern moving, as the phase shift is altered because of the change in path length of one of the beams. As we explained in section 2.3 and graphically showed in Figure 5, the intensity at the beam stopper is extremely sensitive to very small variations in the path length, so even very small changes in the length of one of the arms result in changes in the interference pattern.

3.4 Experiment 4

3.4.1 Set-Up

We now use the Michelson interferometer to measure the frequency separation between the laser modes by constructing a visibility curve. The setup is mostly the same as in experiment 3, but with the spatial filter and beam expander system removed, and a -25 mm diverging lens inserted in between the beam splitter and the beam stopper in order to magnify the interference fringes. We alter the length of the arm containing M2 by moving the mirror using the translation stage and also moving the translation stage itself in order to acquire data at multiple positions. At each position of M2, we take a picture of the interference fringes using the camera of a Samsung Galaxy S7 smartphone, and analyze the intensities using the Python SciPy library.

3.4.2 Results and analysis

Figure 15: Fringe pattern at location of maximum visibility.

Figure 16: Fringe pattern at location of minimum visibility.

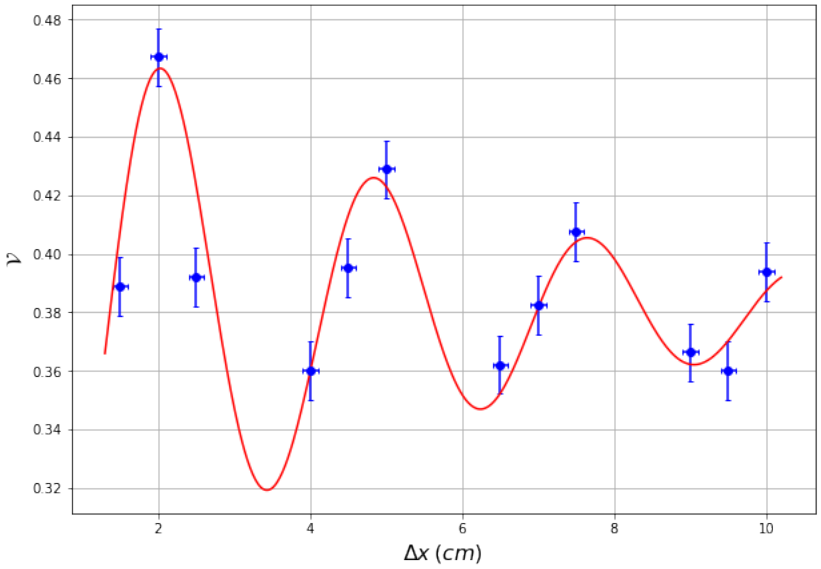

Figure 17: Visibility curve derived from measurements, plus fit using model given in (19).

Figures 15 and 16 show digital images of the interference patterns at the locations of maximum visibility ($\Delta x = 0$ cm) and minimum visibility ($\Delta x = 9.5$ cm), respectively. Figure 17 shows the visibility curve obtained and a fit using the model given in (19). Note that we have performed the fit starting at $\Delta x = 1.5$ cm instead of at $\Delta x = 0$ cm in order to simplify the fitting model. We assume a standard error for the visibility values of 0.1, and a standard error for Δx of 0.1 cm, mainly due to the difficulty in locating exactly the location of $\Delta x = 0$. We find a best fit parameter for the frequency of the sine wave of $\gamma = 224 \pm 8$ m^{-1}, which by equation (20) gives a value for the frequency separation of the modes of $\Delta\nu = 1.33 \pm 0.05$ GHz. This in turn implies a laser cavity length of $L = 11.2 \pm 0.4$ cm, which

is consistent with our expectations of $L \approx 10$ cm. This is a remarkably good result, especially due to the approximate fitting model that we have used; more accurate results can be obtained if the ratio of the intensities between the laser modes is known, or by performing a more sophisticated analysis that numerically solves the integral that describes the flux distribution of the laser light for different values of the ratio, in order to fit for both the ratio and the frequency separation at the same time.

3.5 Experiment 5

3.5.1 Set-Up

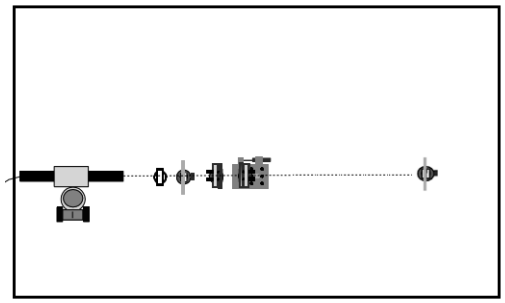

Figure 18: Setup for experiment 5. Modified from original obtained from [6].

In this last experiment, we construct a Fabry-Perot interferometer and study its fringes. We set up a spatial filter with a 25 mm lens and a pinhole, as we did in previous experiments, and then mount two identical flat interference plates at a distance of $d = 5 \pm 0.2$ cm from each other, and ~ 7 cm away from the pinhole. We align the orientation of the plates such that it is possible to observe circular fringes at the beam stopper placed some distance away from the cavity. We now observe the behavior of the fringes under different circumstances. We first blow air through the space separating the plates, then bend one of the posts holding one of the interference flats, and introduce a polarizer in between the laser and the 25 mm lens and observe what happens to the fringes when we rotate the polarizer. Finally, we measure the interferometer's power reflection coefficient R by using a photosensor to find the ratio of the transmitted intensity to the incident intensity, and then using the relationship $R = 1 - T$. We assume that the interferometer has negligible absorptance.

3.5.2 Results and analysis

Figure 19: Fabry-Perot fringes observed during the experiment. The big shadow to the right of the central spot is due to a pencil mark in the beam stopper itself.

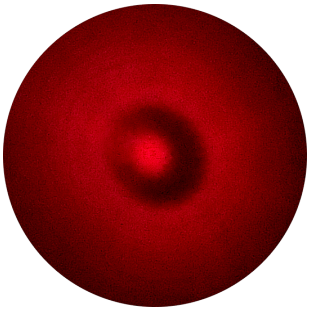

Figure 20: Another picture of the Fabry-Perot fringes.

Figures 19 and 20 show two different images of the Fabry-Perot fringes that were produced during the experiment. Our measurement of the transmission coefficient yielded a value for the reflection coefficient of $R = 0.99827 \pm 0.00005$, which results in a finesse $\mathcal{F} = 1820 \pm 50$, a minimum resolvable frequency separation of $(\Delta v)_{min} = 1.65 \pm 0.08$ MHz, and a free spectral range $(\Delta\nu)_{FSR} = 3.0 \pm 0.1$ GHz. This implies that, in principle, we should be able to observe interference fringes for the each of the laser modes, since the minimum resolvable frequency is three orders of magnitude less than the actual frequency separation $\Delta\nu$ that was measured in experiment 4.

Blowing air through the space in between the plates blurs the fringes, because it introduces a variable refractive index that chaotically alters the phase difference of the transmitted waves, much like what happened when we blew the Airoduster in one of the arms of the Michelson interferometer. Bending a post makes the fringes disappear, since it disrupts the the plates alignment, and this type of interferometer is extremely sensitive to misalignments. In theory, changing the polarization of the incident light should have interesting effects on the fringes. The laser has three modes, but only two of those interfere with each other, because the third mode has a polarization that is perpendicular to that of the other two, and two waves of opposite polarizations cannot mutually interfere. The frequency separation that we measured in experiment 4 was the frequency separation of the two modes with equal polarization. Thus, positioning a polarizer in between the laser and the spatial filter and rotating it such that its transmission axis is perpendicular to the polarization axis of the two modes should, in theory, make two sets of fringes disappear, leaving behind only one set of fringes corresponding to the third mode that has a polarization in the direction of the transmission axis of the polarizer. This effect, however, was not observed. There are two possible reasons for this. The first one is that the resolution at which we were able to observe the fringes was not ideal, as Figures 19 and 20 show. We can observe the fringes produced by the main mode, which has the largest intensity; but the separation between the fringes is small, the fringes have a non-zero width, and the difference in intensity between the modes is supposed to be large, which means that it is very hard to observe the fringes corresponding to the other modes. Instead, what we observed when we rotated the polarizer was that the fringes would blur and become clearer at certain intervals, and nothing else. The same effect was observed during laser warmup, where we know that the intensity transmitted by the polarizer changes rapidly

and by large amounts, as we have observed that behavior in previous labs. The other possible reason for the null result is that the laser light is supposed to be randomly polarized. This means that, even if we assume that two modes are always polarized in the same direction, and the other one is always polarized perpendicularly with respect to the other two, there is no reason why we should expect to be able to make two sets of fringes disappear at a certain angle of the polarizer: the polarization of the modes is still expected to randomly vary at very fast intervals, so the angle between the incoming light and the polarizer's transmission axis will never be the same for detectable periods of time. If this weren't the case, it should be possible to block most of the laser light just by setting the polarizer at a specific angle. The transmission of the Fabry-Perot cavity is certainly sensitive to the incoming polarization, but this sensitivity should be small at angles near to normal incidence, so we expect this factor to be negligible in our setup.

4 Conclusions

We have performed a series of experiments to investigate the phenomenon of interference, in the context of classical electromagnetism. We have used interference effects to measure the thickness of a cover glass, estimate the wavelength of laser light, and observe the frequency separation between laser modes. All experiments have been successful to varying degrees. Better results could potentially be obtained by increasing the accuracy of certain measurement procedures. For instance, experiment 1 could produce more accurate results if we used a very large rotation stage in order to measure deflection angles, or performed the experiment in a larger table with holes separated by less distance. In experiment 2, there is plenty of room for improvement in the measurement of the quantities Δy and a', which could potentially be achieved by using a razor blade and a photosensor in a manner similar to what was done in project 3 in order to measure the laser beam's width. Experiment 4's results would be more accurate if more data had been taken for the visibility curve, and a more sophisticated numerical analysis had been performed in order to find a better fitting model. Finally, using a higher resolution camera would have been helpful in order to better analyse the fringes produced by the Fabry-Perot interferometer.

5 Acknowledgements

The author of this work would like to acknowledge the help received from his lab partner, Juliette Fropier, throughout the data gathering process. I would also like to acknowledge the help provided by our professor, Mukund Vengalattore, and our TA, David Moreau, during lab time.

References

[1] van der Walt, S., et al. *The NumPy Array: A Structure for Efficient Numerical Computation*, Computing in Science & Engineering, 13, 22-30, 2011.

[2] Lebigot, E.O. *Uncertainties: a Python package for calculations with uncertainties*, http://pythonhosted.org/uncertainties/

[3] Hecht, E. *Optics, 5th edit.*, Pearson Education Limited, 2017.

[4] Born, M. & Wolf, E. *Principles of Optics, 7th (expanded) edit.,* Cambridge University Press, 1999.

[5] Bodenschatz, E., et al. *Modern Experimental Optics Laboratory Manual*, Cornell University Physics Department 2016.